A more accurate three-dimensional grain growth algorithm

Emanuel A. Lazar [a],*, Jeremy K. Mason [b], Robert D. MacPherson [b], David J. Srolovitz [c]

[a] *Program in Applied and Computational Mathematics, Princeton University, Princeton, NJ 08544, USA*
[b] *School of Mathematics, Institute for Advanced Study, Princeton, NJ 08540, USA*
[c] *IHPC, 1 Fusionopolis Way, 16-16 Connexis, Singapore 138632, Singapore*

Abstract

In a previous paper, the authors described a simulation method for the evolution of two-dimensional cellular structures by curvature flow that satisfied the von Neumann–Mullins relation with high accuracy. In the current paper, we extend this method to three-dimensional systems. This is a substantial improvement over prior simulations for two reasons. First, this method satisfies the MacPherson–Srolovitz relation with high accuracy, a constraint that has not previously been explicitly implemented. Second, our front-tracking method allows us to investigate topological properties of the systems more naturally than other methods, including Potts models, phase-field methods, cellular automata, and even other front-tracking methods. We demonstrate this method to be feasible in simulating large systems with as many as 100,000 grains, large enough to collect significant statistics well after the systems have reached steady state.
© 2011 Acta Materialia Inc. Published by Elsevier Ltd. All rights reserved.

1. Introduction

Current knowledge of grain growth in polycrystalline materials relies on a combination of experimental observations of grain growth microstructures, developments in kinetic theory, and more recently, simulations of microstructural evolution. This understanding is limited by the difficulty of experimentally accessing the details of a three-dimensional microstructure, by the anisotropy of properties that govern grain boundary motion (e.g. grain boundary energy and mobility), and by impurities and inhomogeneities in real materials (i.e. the presence of a solute species or crystalline defects). Hence, despite recent advances in three-dimensional microscopy [1,2], in characterizing the anisotropy of grain boundary energies and mobilities [3,4], and in analyzing the effects of impurities [5,6], the importance of theory and simulations developed for simplified and idealized microstructures cannot be overstated. Indeed,

a model that assumes material isotropy, a grain boundary motion governed only by interfacial thermodynamics (the Gibbs–Thomson relation), and the absence of impurities provides fertile ground for investigating basic features of the complicated process of grain growth. As an example, these idealizations have permitted an exact solution for the rate of growth of any given grain within a microstructure. This was done first in two dimensions by von Neumann [7] and Mullins [8], and more recently in three and higher dimensions by MacPherson and Srolovitz [9].

Nonetheless, even with this idealized model and the accompanying exact solutions, our understanding of the properties of the evolving microstructure remains rudimentary. Difficulties with developing a theory of the broader microstructure arise principally in understanding the interactions between grains and from the many degrees of freedom of a grain boundary network in three dimensions. As an alternative, simulations have provided important insights into the mechanisms and energetics of grain growth [10,11], but contemporary simulation methods do not rigorously adhere to the same assumptions of isotropy

* Corresponding author. Tel.: +1 412 613 7271; fax: +1 609 258 1735.
  E-mail address: lazar@princeton.edu (E.A. Lazar).

and curvature-driven grain boundary motion that have proven instrumental in developing the theory for individual grains. In this paper, we present a new method for simulating grain growth in an idealized microstructure that is consistent with these assumptions. This new method for three-dimensional grain growth obeys the exact relation for the rate of growth of every grain, is more accurate and more efficient than prior simulations, and is capable of investigating microstructural properties previously overlooked. An example of a simulated three-dimensional microstructure is illustrated in Fig. 1.

One of the most frequently used simulation methods is a Monte Carlo Potts model [12–14], which represents grains as ensembles of lattice points sharing the same label. Evolution of the structure is performed by allowing the label of a lattice point to change probabilistically based on an energy that is a function of the labels of neighboring points. The implementation of this method is relatively straightforward, without the need to explicitly distinguish between the interior of grains and the grain boundaries or explicitly implement topological changes in the grain boundary network. While this approach has been used to simulate polycrystalline systems with more than 2,000,000 grains [15], certain questions remain. The discretization of the structure into volume elements limits the resolution of the simulation and often introduces spurious anisotropy (e.g. facet formation on surfaces commensurate with the lattice) [12,16]. Furthermore, the resulting microstructures do not rigorously maintain the angles along grain boundary junctions as demanded by thermodynamics. Finally, the discretization inherent to this method introduces to the microstructure a length scale associated with the underlying numerical lattice (unrelated to the atomic lattice length scale), and makes measuring topological and geometrical quantities difficult [17].

A closely related approach is the cellular automata model [18,19]. This model inherits the simplicity of the Potts model's discrete lattice structure and labeling system, but allows a wider range of energetic conditions to be introduced into the switching probabilities of the labels. Recent work has been able to simulate systems with roughly 30,000 grains [20]. Cellular automata models have many of the same limitations as the Potts model though, including the possibility of faceting and lattice pinning due to the lattice-based discretization of the microstructure.

Another approach developed for three-dimensional systems is the phase-field method [21,22], where a smoothly varying order parameter is defined for every grain orientation. A given grain occupies the region where the corresponding order parameter is 1 and all other order parameters vanish. The energy of the system depends on the values and gradients of all the order parameters, and the system is evolved using a non-conserved Ginzburg–Landau equation [23]. While this procedure allows for the incorporation of sophisticated energetics, a large number of coupled nonlinear differential equations must be numerically solved at every time step [24]. Furthermore, this method requires a finite grain boundary width (rather than the sharp boundaries for the Potts and cellular automata models), implying that the thermodynamic constraint on the angles at which grain boundaries meet is relaxed. This finite width is a result of the requirement that gradients of the order parameters be small, and the consequent requirement for a very fine discretization of the microstructure [25]. The resulting demands for computational resources currently limit phase-field methods to systems containing 30,000 grains [26].

The final primary approach to simulate three-dimensional grain growth are various front-tracking methods in which two-dimensional grain boundaries are explicitly represented. Most front-tracking simulations are either "vertex models", which follow the motion of only the quadruple points (where four boundaries meet) [27], or are only slightly more refined, and allow for nonplanarity of the faces by introducing a further node in the center of a face [28–30]. These methods provide only coarse discretizations of the grain boundary network and cannot adequately capture the curvature of the interfaces. A more severe limitation of these models is their inability to represent two-edged faces and three-faced grains, entities that certainly arise in physical systems [31,32].

Apart from vertex models, several other implementations of front-tracking methods exist. A recent simulation [33] uses Brakke's Surface Evolver [34] to construct and evolve grain boundaries with a finer discretization that is more able to reflect the boundary curvature, an essential feature of grain growth. While Surface Evolver is able to handle many of the topological transitions that arise in the grain boundary network, it is currently unable to describe others that routinely occur during normal grain growth. When such transitions occur, the microstructure must be manually readjusted to account for the change. A separate front-tracking approach [35] uses finite-element methods to provide an elegant, accurate discretization of
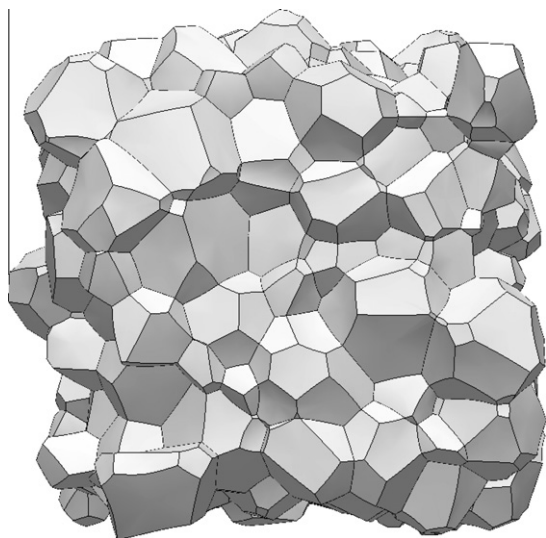

Fig. 1. A system of 250 grains.

the microstructure. However, the computational expense associated with preserving the mesh quality has limited these simulations to fewer than 5000 grains.

All front-tracking methods benefit from the explicit representation of the grain boundary network, facilitating calculations of topological and geometrical quantities of interest. This creates certain challenges though, including the need to explicitly address and program all topological changes that occur during system evolution. While the evolution of two-dimensional microstructures involves only the disappearance of grains and edge-flips, in three dimensions the disappearance of grains as well as the disappearance and creation of edges and faces must be implemented. This topological complexity, along with the resources necessary to represent and evolve these structures, has limited previous work in this area to systems of 6000 grains [33,36,37].

Of particular note is that all of these prior simulation methods generally fail to satisfy the MacPherson–Srolovitz relation [9], which extends the classic von Neumann–Mullins relation to three dimensions and governs the rate of change of volume of each grain. Even front-tracking methods, which prescribe velocities of individual nodes according to local curvatures and which increasingly approximate the correct solution with refinement of the surface mesh, fail to satisfy the MacPherson–Srolovitz relation for any finite discretization. It is unclear how the error introduced by these method impacts the microstructures that appear in the steady state.

In a previous paper [38], the authors introduced a front-tracking method for two-dimensional grain growth that accurately satisfies the von Neumann–Mullins relation [7,8]. In what follows, we extend this method to three dimensions, maintaining the same high level of accuracy in satisfying the exact MacPherson–Srolovitz relation [9]. Specifically, the error in displacement of the nodes during a time step Δt is of the order $O(\Delta t^2)$, and the relative error in the rate of change of the volume of a grain from the discretization of the surface mesh is found to be small. Furthermore, our implementation allows us to model large systems, observe them as they evolve into steady-state microstructures, and examine many of their topological and geometrical properties in a very straightforward manner. In this paper, we provide compiled statistics from eight grain growth simulations, each beginning with 100,000 grains, representing a substantial increase in the size and accuracy of the simulations beyond the largest currently appearing in the literature.

2. Data structure and algorithm

The fundamental equation that governs normal grain growth in three-dimensional isotropic polycrystalline materials is the MacPherson–Srolovitz relation [9] which describes the volume evolution of individual grains:

$$\frac{dV(D)}{dt} = -2\pi M\gamma\left(\mathcal{L}(D) - \frac{1}{6}\mathcal{M}(D)\right),\tag{1}$$

where $V(D)$ is the volume of grain D, $\mathcal{L}(D)$ is a one-dimensional measure of the grain size called the mean width, and $\mathcal{M}(D)$ is the sum of the lengths of all triple edges (along which three grains meet) of the grain; M and γ are constants describing the grain boundary mobility and grain boundary energy, respectively. This result is exact for normal grain growth in isotropic polycrystalline materials.

The algorithm described below accurately evolves a triangulation of the grain boundary network, but allows considerable variation in the triangulation used. This algorithm requires that every grain be represented as a closed collection of faces (two-dimensional grain boundaries). Every face is composed of a collection of triangular facets with face nodes on the interior of the face and a number of boundary nodes around its perimeter. Boundary nodes located at points where four grain meet are called vertex nodes, while boundary nodes located at points where three grains meet are called edge nodes. Line segments that connect adjacent boundary nodes are triple edge segments, while line segments connected to at least one face node are regular edge segments.

The general algorithm for evolving the microstructure involves two parts. First, we calculate the appropriate displacements for all nodes at every time step and move the nodes of the triangulation accordingly. Second, we implement topological changes that occur while the system evolves, such as the disappearance of edges and faces. We first describe the node displacements. The analytic solution for the volume evolution of each grain is given by Eq. (1). We discretize the time and volume variables in this equation and solve for the change in grain volume $\Delta V(D)$:

$$\Delta V(D) = -2\pi M\gamma\left(\mathcal{L}(D) - \frac{1}{6}\mathcal{M}(D)\right)\Delta t.\tag{2}$$

Next, we localize this equation for each node of the grain. That is, for each grain D we calculate "local" versions of $\mathcal{L}(D)$ and $\mathcal{M}(D)$ for every node, and then change the volume of grain D near each node by an appropriate amount. Done carefully, this will ensure that Eq. (2) will be satisfied for every grain at every time step with an error proportional to the square of the time step Δt.

We briefly explain the terms $\mathcal{L}(D)$ and $\mathcal{M}(D)$. The first is a linear measure known as the mean width which measures the total mean curvature on the surface of a grain; this is a key quantity in describing systems that evolve via mean curvature flow.[1] Because our discretized grains are piecewise flat, the mean width $\mathcal{L}$ reduces to a sum over all edge segments of a grain. If e_i is the length of the ith edge segment, and α_i is the exterior angle at that edge segment with respect to the same grain, then:

---

[1] More information about the mean width can be found in Ref. [9], and especially in its Supplementary Information. The interested reader can find there a more elaborate definition of the term, as well as many helpful examples. To date, there is no standard reference on this subject.
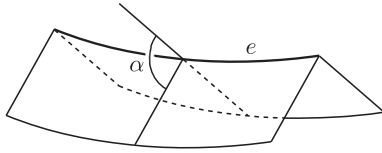
Fig. 2. Illustration of an exterior angle α with respect to the grain sitting below the two faces for a typical edge e.

$$\mathcal{L}(D) = \frac{1}{2\pi} \sum_i e_i \alpha_i, \tag{3}$$

where i is indexed over all edge segments (both regular and triple) of grain D. Fig. 2 shows the exterior angle α of a typical edge e.

The second term $\mathcal{M}(D)$ measures the length of all triple edges around grain D, i.e. all edges at which three different grains meet. If e_j is the length of a triple edge segment j of grain D, then:

$$\mathcal{M}(D) = \sum_j e_j, \tag{4}$$

where j is indexed only over triple edge segments of the grain. In this description, $\mathcal{L}(D)$ and $\mathcal{M}(D)$ are then defined as sums over the edge segments of a grain. However, we can also define these quantities as sums over the nodes of a grain. We can define "local" versions of $\mathcal{L}(D)$ and $\mathcal{M}(D)$ at every node n of a grain D:

$$\mathcal{L}_n(D) = \frac{1}{4\pi} \sum_i e_i \alpha_i, \tag{5}$$

$$\mathcal{M}_n(D) = \frac{1}{2} \sum_j e_j, \tag{6}$$

where i is indexed over all edge segments (both regular and triple) of grain D that are incident with a node n, and j is indexed only over the respective triple edge segments. We can then rewrite Eqs. (3) and (4) as sums over nodes: $\mathcal{L}(D) = \sum_k \mathcal{L}_k(D)$ and $\mathcal{M}(D) = \sum_k \mathcal{M}_k(D)$, where k is indexed over all nodes of a grain. Because the faces of our grains are piecewise flat, the amount by which the volume of a grain will change by moving node n by d$\boldsymbol{n}$ is:

$$\Delta V_n(D) = \frac{1}{6} \sum_{i,j} (e_i \times e_j) \cdot \mathrm{d}n, \tag{7}$$

where $\boldsymbol{e}_i$ and $\boldsymbol{e}_j$ are all ordered pairs of consecutive edge vectors pointing from a node n to its neighboring nodes, ordered clockwise with respect to an outward-pointing normal; here no distinction is made between regular and triple edge segments.

We can now use these "local" versions of $\mathcal{L}(D)$, $\mathcal{M}(D)$, and $\Delta V(D)$ to define a local version of Eq. (2):

$$\Delta V_n(D) = -2\pi M\gamma \left(\mathcal{L}_n(D) - \frac{1}{6}\mathcal{M}_n(D) \right) \Delta t. \tag{8}$$

Since all terms on the right are determined, we have only to substitute for $\Delta V_n(D)$ using Eq. (7) and solve for d$\boldsymbol{n}$ to find a displacement that will satisfy the MacPherson–Srolovitz relation locally at every node of the grain D.

The actual motion of a node is given by three unknown spatial variables. The grains adjacent to face nodes, edge nodes and vertex nodes provide two, three and four constraining equations of the type described above, respectively. Not all of these constraints are independent though, since the volume of all grains incident with a node should be conserved with that node's displacement. This leaves three unknowns and one, two and three constraints for each face node, edge node and vertex node, respectively. That is, there remains one degree of freedom when moving edge nodes and two degrees of freedom when moving face nodes.

Node displacements are decomposed into two parts. First, we move nodes by distances that appropriately change the volumes of the adjacent grains. Specifically, we move each face node in the unique direction that minimizes the magnitude of the node displacement; this direction is roughly perpendicular to the face. Likewise, we move each edge node in the unique direction that minimizes the magnitude of that node displacement; this direction is orthogonal to the line segment connecting the edge node with the two neighboring boundary nodes. The direction of the vertex node displacement is completely determined. Because each individual displacement satisfies the local, discretized version of the MacPherson–Srolovitz relation (Eq. (8)), the only error involved in these displacements are "interference" errors that result from the simultaneous movement of adjacent nodes. In the next section we show that the this error is small.

In order to maintain numerical stability, we then move each face node as close as possible to the center of mass of the boundary of the adjoining triangles and each edge node as close as possible to the center of its two adjacent boundary nodes. These displacements help to keep face nodes from wandering towards face boundaries and edge nodes from becoming too close to one another, both of which can cause instability. While individual face nodes and edge nodes may be moved in a way that preserves the volumes of the two or three neighboring bodies, the simultaneous motion of all of the face nodes and edge nodes in this manner creates further "interference" errors identical to the ones mentioned above. Since this error is small, we believe that it is outweighed by the improvement in numerical stability.

At first sight, the displacements described in this section may not resemble motion by mean curvature, since we do not attempt to move nodes in their normal directions and with magnitudes proportional to their local curvature. Indeed, a more naive approach may attempt to define a normal direction at every node, and move each node in that direction by an amount proportional to the mean curvature at that point. The difficulty is that while this method adequately describes the necessary displacements at points commensurate with the nodes, it does not adequately describe the motion of the other points of the triangulation. In the current method, rather than considering the velocities of a finite number of points and moving the surface
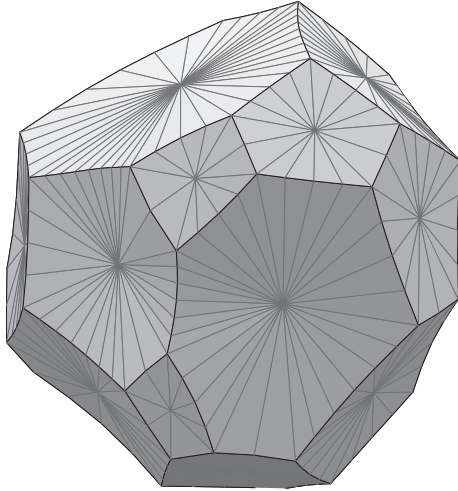
Fig. 3. A single grain.

Fig. 4. A volume element associated with a triangular facet on the grain boundary.

as those points require, we consider the way in which the volume of a grain changes with the movement of entire triangular facets. This allows us to accurately satisfy the exact MacPherson–Srolovitz relation without resorting to arbitrarily refined surface meshes.

Our simulations in particular use a single face node located in the center of a given face to simplify the implementation and to reduce the computational requirements. An example of a single, discretized grain from our simulations is given in Fig. 3. Edge nodes are added to make the discretization smoother, and occasionally removed when neighboring ones become too close. Two adjacent boundary nodes and a neighboring face node then determine a small, flat triangular facet of a face, as seen in the figure.

3. Error analysis

We now consider the error associated with evolving a given triangulation one time step by the above equations. This error is measured by comparing the volume change of a grain in one time step to that predicted by the exact solution for a grain of the same shape, the discretized Mac-Pherson–Srolovitz relation (Eq. (2)). We demonstrate that our method produces errors from the discretization of time that are proportional to $(\Delta t)^2$ to leading order, independent of the triangulation used.

Consider a simple tetrahedron such as that shown in Fig. 4. Imagine one of its corners, c, placed in the center of a discretized grain, and the other three corners, v_1, v_2 and v_3, placed at the three corners of a triangular facet of that grain. Every grain can be decomposed into a finite number of these tetrahedra, with one tetrahedron associated with each triangular facet of the grain.

Before moving any of the vertices, the volume of the tetrahedron can be determined from the edge vectors e_1, e_2 and $e_3 : V = \frac{1}{6}e_1 \cdot (e_2 \times e_3)$. If we only move v_1 by $dv_1\Delta t$, then the volume would change by $\frac{1}{6}(e_2 \times e_3) \cdot dv_1\Delta t$. Likewise, if we only move v_2 or v_3, then the volume would change by
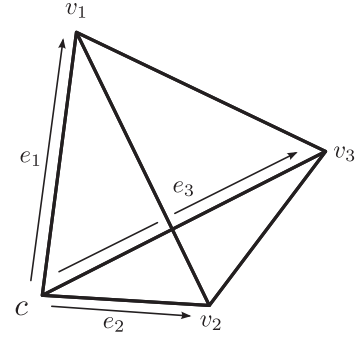
$\frac{1}{6}(e_3 \times e_1) \cdot dv_2\Delta t$ or $\frac{1}{6}(e_1 \times e_2) \cdot dv_3\Delta t$, respectively. An "exact" solution involved in moving all three vertices should then change the volume by $\Delta V(D) = \frac{1}{6}[(e_2 \times e_3) \cdot dv_1 + (e_3 \times e_1) \cdot dv_2 + (e_1 \times e_2) \cdot dv_3]\Delta t$. However, if we move all three vertices at the same time, we find that the volume actually changes by $\Delta V_a(D) = \frac{1}{6}(e_1 + dv_1\Delta t) \cdot ((e_2 + dv_2\Delta t) \times (e_3 + dv_3\Delta t)) - \frac{1}{6}e_1 \cdot (e_2 \times e_3)$. The difference between these two numbers is the "interference" error involved in these node displacements:

$$\Delta V_a(D) - \Delta V(D) = \frac{1}{6}e_1 \cdot (dv_2 \times dv_3)\Delta t^2$$
$$+ \frac{1}{6}e_2 \cdot (dv_3 \times dv_1)\Delta t^2$$
$$+ \frac{1}{6}e_3 \cdot (dv_1 \times dv_2)\Delta t^2$$
$$+ \frac{1}{6}dv_1 \cdot (dv_2 \times dv_3)\Delta t^3. \tag{9}$$

Since the e_i and dv_i are independent of Δt, the error for these overlapping displacements is, to leading order, proportional to Δt^2. Since each grain can be decomposed into a finite number of these tetrahedra, the total error for each grain is merely a sum of these interference errors and is thus also of order $O(\Delta t)^2$.

One way to visualize the magnitude of the error involved in this method is by plotting $\Delta V/\Delta t$ for each grain against the rate of change of the volume predicted by the MacPherson–Srolovitz relation. Fig. 5 shows these values for the current method and for Surface Evolver [34], a prominent front-tracking program that is used for grain-growth simulations [39,33]. It is clear from these data that Surface Evolver produces much larger errors from the discretization of time than does our method.

There remains the question of the error introduced by the triangulation itself, i.e. from the discretization of space. Generally speaking, for a triangulation where the linear size s of the individual triangles is small and the triangles are equiaxed, the error in the mean width introduced by discretizing a continuous grain D scales as $(s/\mathcal{L}(D))^2$ [9]. Regrettably though, a precise calculation of this error is not possible since an exact description of the surface of any grain that occurs during normal grain growth is not
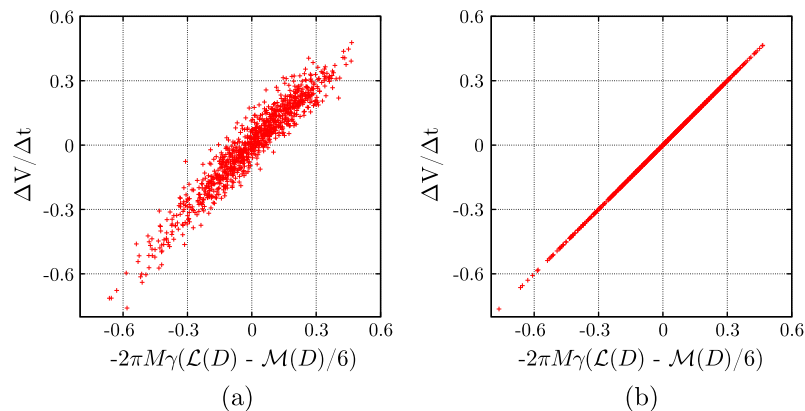
Fig. 5. The rate of change of volume vs. the rate of change of the volume predicted by the MacPherson–Srolovitz relation for (a) Surface Evolver and (b) the current method. Data is collected from one time-step in a system with 1000 grains.

available. As evidence of the difficulty involved, suppose that the limiting shape of the faces of a two-faced grain in a physical system are spherical caps. Consider that in an infinitesimal time interval, every infinitesimal piece of the spherical cap moves an equal amount toward the center of the coincident sphere. A geometric construction reveals that this would cause the dihedral angle of the faces of the grain to depart from $2\pi/3$, despite the requirement that the dihedral angle be an invariant of the physical system. Therefore, a grain with spherical caps does not evolve in a self-similar fashion during normal grain growth, and cannot be the limiting shape of the two-faced grain.

Nevertheless, a spherical cap may be a reasonable approximation for a continuous face in a physical system [40]. Using our triangulation, the discrete analog to this continuous face is a pyramid over a polygonal base. The relative error introduced by our triangulation is estimated by comparing the integrals of the mean curvature over the continuous face and the corresponding discretized face, and is found to be about one percent. We stress that this is a consequence of the triangulation, and not of the algorithm, which is entirely amenable to the use of a finer surface mesh. Furthermore, this error in our implementation is offset by the fact that our choice has allowed us to perform a front-tracking simulation containing more than a factor of 10 more grains than other comparable simulations [33,36,37]. Finally, we point out that the same error is not generally reported for other simulation methods, and therefore may not be compared with ours. Further details of the relevant calculation may be found in the Supplementary material.

4. Topological changes

Aside from calculating displacements for all nodes at every step we must also describe the appropriate topological changes that occur during coarsening, namely the disappearance of grains and the disappearance and creation of edges and faces. In three-dimensional systems, all typical topological events can be decomposed into combinations of five elementary topological changes: the disappearances of (a) edges, (b) triangular faces, (c) two-sided faces, (d) tetrahedral grains and (e) three-faced grains.[2] These events occur when the length of an edge, the area of a face or the volume of a grain approaches zero. Since none of these quantities can be negative, we are forced to make appropriate changes in the system by deleting these entities and creating new ones in their place. Fig. 6 illustrates these five topological changes.

Although we did not initially expect them, the occurrence of two-sided faces and three-faced bodies during normal grain growth is widely reported in the literature, including in numerous experimental studies [31,32,41] and several recent simulations [33,36,37]. Curiously, these topological events do not seem to appear in some otherwise detailed discussions of three-dimensional grain growth, including Ref. [42].

The two most frequent changes that occur in an evolving system are the disappearance and creation of edges and triangular faces. When edges disappear new triangular faces are created, and when triangular faces disappear new edges are created. In this sense these changes can be considered duals and are "reversible"; the other three topological changes are not reversible. As for the occurrence of more complicated topological events, consider the disappearance of a grain that has two faces with two sides and two faces with four sides. Such a grain is collapsed by first removing a two-sided face. The remaining grain, which has three two-sided faces, is then removed. This topological trajectory is illustrated in Fig. 7. All topological events that we have observed in the evolution of our systems may be decomposed in this manner, meaning that the algorithm is simplified by requiring only a small number of topological events to be implemented. Since the details of the code are lengthy and depend on the triangulation, we do not describe them here.

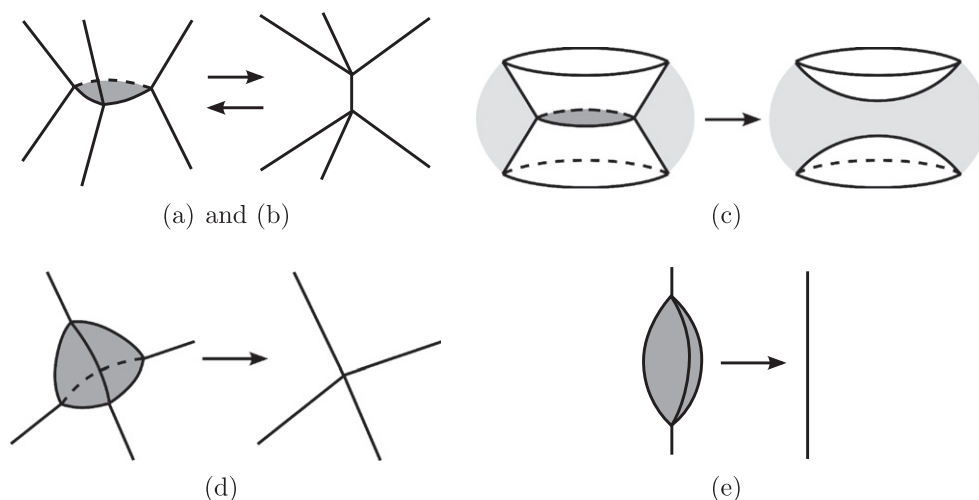[2] These five could be further decomposed into combinations of only three fundamental events.

Fig. 6. Five basic topological changes: (a) an edge disappears and becomes a triangular face; (b) a triangular face disappears and becomes an edge; (c) a two-sided face disappears and two neighboring faces merge; (d) a grain with four triangular faces disappears into a vertex; (e) a grain with three two-sided faces disappears into a triple-edge.
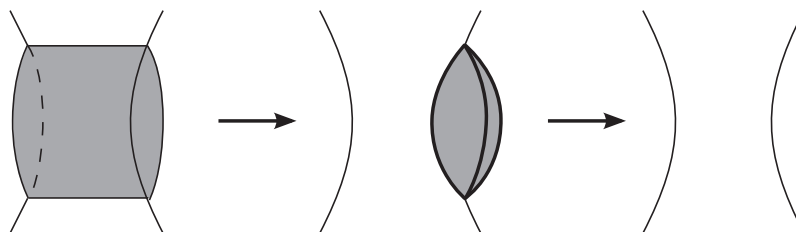

Fig. 7. This quickly shrinking grain is removed in two steps: first a two-sided face is removed, then the remaining three-faced grain is deleted.

5. Microstructural evolution

We now report on the simulation results from our implementation of the algorithm described above. The initial condition for all of our simulations are Voronoi tessellations of 100,000 points randomly distributed in a unit cube with periodic boundary conditions. Setting the length of the unit cell to L, we measure time in dimensionless units of $L^2/M\gamma$, where M and γ are the grain boundary mobility and energy, respectively (as described above).

In the initial Voronoi tessellation, all grains have flat faces and straight edges. The evolution of a typical microstructure is illustrated by still images in Fig. 8, and by an animation in the Supplementary material. After a short time, the faces and edges begin to curve: angles between adjacent faces at triple edges quickly approach $2\pi/3$ and the angles between triple edges at vertex nodes approach the tetrahedral angle $\arccos(-1/3) \approx 109.5°$. The microstructure gradually coarsens over time, resulting in fewer grains and a larger average grain size. Fig. 9 shows that the average grain volume $\langle V \rangle$ increases linearly with $t^{3/2}$ after the initial transient. Assuming that the microstructure remains in the steady state, this behavior can be derived analytically using dimensional analysis [43].

Finally, an animation showing the evolution of a single three-dimensional grain is available in the online suppplemental material to this paper. Many of the topological changes described in Section 4 may be readily identified as the grain shrinks.

6. Steady state

During grain growth the microstructure evolves toward a statistically self-similar state, i.e. a state in which properties are statistically time invariant up to a change in scale. One way of observing this process is by observing scale-independent properties as they relax toward asymptotic, steady-state values. Figs. 10 and 11 show how the average number of faces per grain $\langle F_G \rangle$ and the average number of edges per face $\langle E_F \rangle$ change as the system evolves. Both of these quantities decrease over time from their initial values, characteristic of the initial state [44], but then asymptotically approach constant values which are characteristic of steady-state grain growth.

A frequent prediction in the literature [45,46,40] is that the average number of faces per grain should be about 13.397 in the steady state, while Coxeter [47] provided some justification that this quantity should be around 13.564. We observe that the average number of faces per grain and edges per face remain fixed in the steady state at 13.769 ± 0.016 and 5.128 ± 0.001, respectively, i.e. close but measurably different from Coxeter's prediction. These

(a) 10,000 grains   (b) 5003 grains   (c) 1998 grains

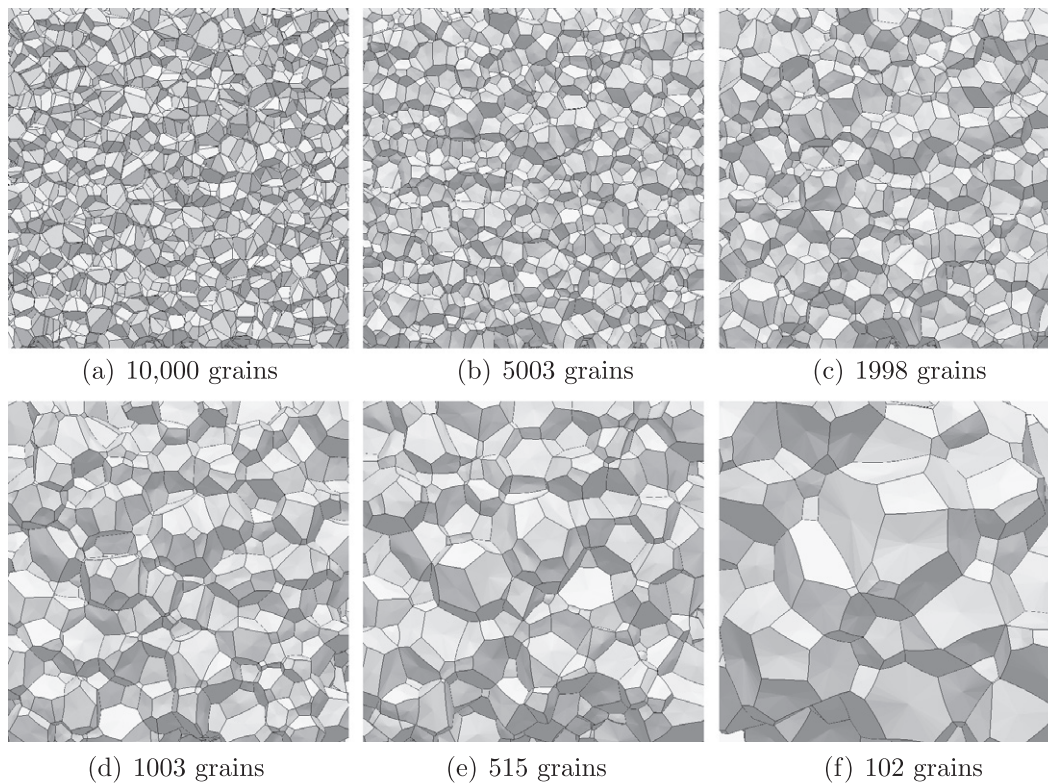(d) 1003 grains   (e) 515 grains   (f) 102 grains

Fig. 8. Temporal evolution of a microstructure using the current method. This microstructure was initialized as a Voronoi tessellation of 10,000 points randomly distributed in the unit cube with periodic boundary conditions. The images were constructed by removing all grains that do not intersect a randomly chosen plane $z = 0$ and imaging the remaining three-dimensional grains.
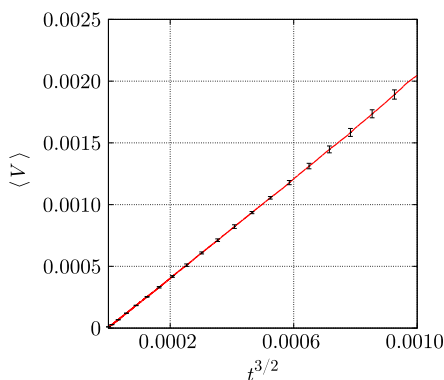

Fig. 9. The average grain volume $\langle V \rangle$ as a function of $t^{3/2}$. Each system began with 100,000 grains; when $t^{3/2} = 0.001$, there remain slightly fewer than 500 grains. Data points are averaged from eight simulations; error bars indicate the standard deviation from the mean.
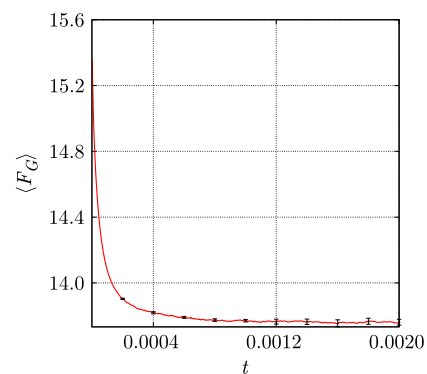

Fig. 10. The average number of faces per grain $\langle F_G \rangle$ decreases as the system evolves away from the initial Voronoi structure. As the system approaches the steady state, this number asymptotically approaches a fixed value close to 13.769 ± 0.016. Data points are averaged from eight simulations; error bars indicate the standard deviation from the mean.

data were obtained from the values at time $t = 0.00125$, when $\approx 10{,}700$ grains remained in each simulation.

Although it is not apparent how to fully characterize steady-state microstructures, we do know the values of several steady-state, scale-invariant properties. For example, the distribution of grain shapes in such a microstructure must have a definite form, as does the distribution of normalized volumes of the grains. Figs. 12–14 show the distribution of edges per face, the distribution of faces per grain, and the distribution of normalized grain volumes. These

results show clearly that the steady-state microstructure is quite different from the initial Voronoi microstructure; this is most apparent when considering the distribution of normalized grain volumes. Note that these data are consistent with earlier simulations of smaller systems using other three-dimensional grain-growth simulation methods [30,33].

The present results represent the largest three-dimensional grain growth simulations performed to date using
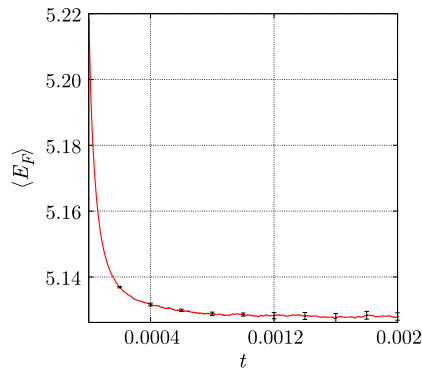
Fig. 11. The average number of edges per face $\langle E_F \rangle$ decreases as the system evolves away from the initial Voronoi structure. As the system approaches the steady state, this number approaches a fixed value, 5.128 ± 0.001. Data points are averaged from eight simulations; error bars indicate the standard deviation from the mean.
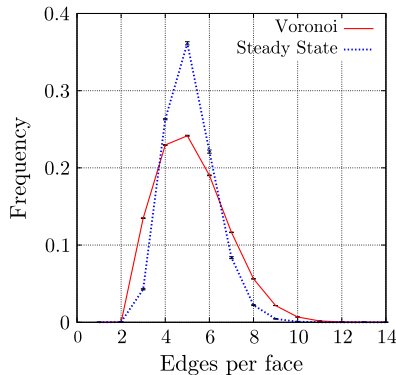

Fig. 14. Distribution of normalized grain volumes $V/\langle V \rangle$ for the initial, Voronoi and steady-state microstructures averaged over eight samples; error bars indicate the standard deviation from the mean.

Fig. 12. Distribution of faces with different numbers of edges from Voronoi configurations and from steady-state microstructures averaged from eight simulations; error bars indicate the standard deviation from the mean.

a front-tracking method. Large data sets are important for several reasons, namely: (i) they ensure that simulations evolve long enough to reach the steady-state microstructure, (ii) they ensure that sufficient grains remain in the steady state to capture reasonable microstructural statistics, and (iii) they ensure that the features of the statistical distributions are sufficiently accurate for comparison with experiments, other simulations and theory. Fig. 13 shows a comparison of the distribution of faces per grain for the present simulation results, a phase-field model [21], two Monte Carlo Potts models [12,48], a front-tracking model [33] and a vertex model [30]. Comparison shows that the current method not only produces significantly smoother curves than the previous methods, but agrees with the mean of the scattered results drawn from smaller simulations.

7. Discussion and conclusions

The MacPherson–Srolovitz relation provides an exact expression for the volume evolution of individual grains in isotropic polycrystalline microstructures. We have developed a simulation method for evolving these structures in a manner consistent with this exact relation. We demonstrate that the present method is simultaneously capable of high accuracy and computational efficiency. Furthermore, the present method accounts for all types of topological reactions that are observed to occur during normal grain growth.

The next step is to use this method to explore more complicated questions regarding the transient period and the steady state. For example, how long do materials take to reach the steady state from different initial conditions? What sort of grain shapes appear in the steady state? For example, what fraction of grains are Kelvin tetrakaidecahedra? What correlation might we expect to find between neighboring grains of various degrees? Our method provides a robust tool for investigating features of the steady-state microstructure which have hitherto been inaccessible by simulation, either from difficulties with identifying geometric features or from limited system size. The
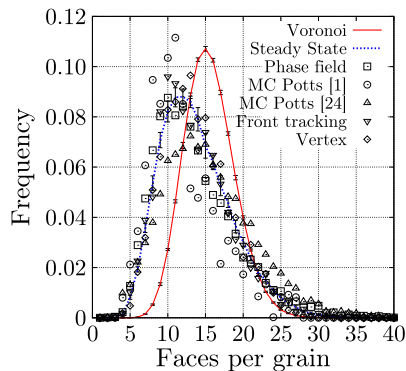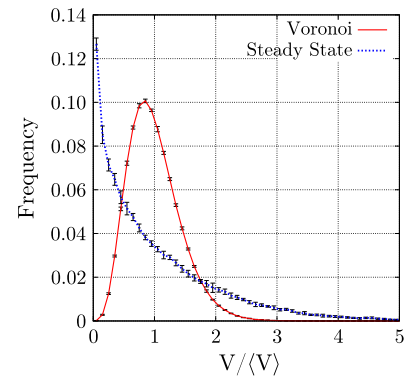

Fig. 13. The distribution of grains with different numbers of faces from Voronoi configurations and from structures evolved using a phase-field method [21], two Monte Carlo Potts models [12,48], a front-tracking method [33], a vertex method [30], and the present results. Data for the Voronoi and steady-state microstructures are averaged from eight simulations; error bars indicate the standard deviation from the mean.
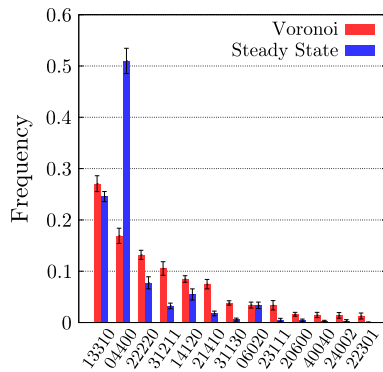
Fig. 15. Distribution of all grains with eight faces in the Voronoi and steady-state systems. Labels along the abscissa indicate how many faces of each type a grain has, e.g. 13310 indicates grains with one three-sided face, three four-sided faces, three five-sided faces, one six-sided face, and zero seven-sided faces. Data is averaged from eight simulations; error bars indicate the standard deviation from the mean. Grain types are ordered based on decreasing frequency of occurrence in the Voronoi microstructure.
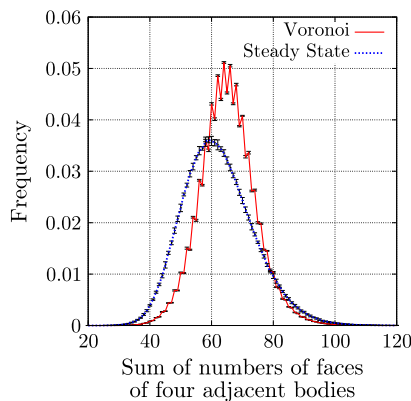

Fig. 16. Distribution of vertices, as characterized by the sum of the numbers of faces of their four adjacent bodies. Data is averaged from eight simulations; error bars indicate the standard deviation from the mean.

eventual goal is to fully characterize the steady state of cellular structures that evolve via mean curvature flow.

While the purpose of this paper is primarily to describe a new approach to simulating normal grain growth that offers significant advantages compared to existing methods, we present a few additional examples of the types of questions that can be addressed with the current method. The data structure inherent to our methodology allows the simple identification of topological features that can be used to determine the distribution of topologically distinct polyhedra within the microstructure. Rather than simply measuring the distribution of faces per grain (as in Fig. 13 and other studies), we are able to specify both the number and types of these faces. For example, Fig. 15 shows the relative frequencies of different eight-faced grains in the Voronoi and steady-state systems. Exactly 14 topologically distinct polyhedra with eight faces can appear in the initial Voronoi tessellation [49]. Two of them have exactly two

three-sided faces, two four-sided faces, two five-sided faces, and two six-sided faces, while the remaining types of grains can be distinguished by the number of faces of each type. After the systems evolve, two-sided faces can appear and more polyhedra are possible, though Fig. 15 excludes grains with two-sided faces. Fig. 15 shows that the distribution of different types of eight-faced grains is much more narrow in the steady state than in the initial Voronoi construction. Indeed, in the steady state a single topological type accounts for over half of all eight-faced grains. Characterizing the topological type of grains more precisely is one example of a way in which our method allows a more complete description of steady-state microstructures.

Another example of a scale-invariant property is the distribution of vertex nodes as characterized by the sum of the numbers of faces of the four neighboring grains, as in Fig. 16. One surprising difference between the Voronoi and the steady-state microstructures is that the Voronoi tessellation apparently prefers vertices with even sums, while the steady-state microstructure shows no such bias.

These two examples are intended to demonstrate the potential our method has for collecting statistically significant measurements of novel topological characteristics of the grain growth microstructure, well within the steady-state regime. While some of our results are similar to those previously collected by other researchers and are included here for the purpose of validation, the results given in this section represent a new class of statistics not heretofore reported for grain growth. We intend to focus on these and other three-dimensional microstructural statistics in a future paper.4pt?>

Acknowledgements

Appendix A. Supplementary material

Supplementary data associated with this article can be found, in the online version, at doi:10.1016/j.actamat.2011.07.052.

References

[1] Konrad J, Zaefferer S, Raabe D. Acta Mater 2006;54(5):1369–80.
[2] Nielsen SF, Lauridsen EM, Jensen DJ, Poulsen HF. Mater Sci Eng A – Struct 2001;319:179–81.
[3] Saylor DM, Mason DE, Rohrer GS. J Am Ceram Soc 2000;83(5):1226–32.
[4] Napolitano RE, Liu S, Trivedi R. Interface Sci 2002;10(2):217–32.
[5] Zou J, Kotchetkov D, Balandin AA, Florescu DI, Pollak FH. J Appl Phys 2002;92:2534.
[6] Liu YL, Primdahl S, Mogensen M. Solid State Ionics 2003;161(1-2): 1–10.

[7] von Neumann J. Written discussion. In: Metal interfaces. Cleveland (Ohio): American Society for Metals; 1952. p. 108–10.

[8] Mullins WW. J Appl Phys 1956;27:900–4.

[9] MacPherson RD, Srolovitz DJ. Nature 2007;446(7139):1053–5.

[10] Srolovitz DJ, Grest GS, Anderson MP. Acta Metall Mater 1985;33(12):2233–47.

[11] Rollett AD, Srolovitz DJ, Anderson MP. Acta Metall Mater 1989;37(4):1227–40.

[12] Anderson MP, Grest GS, Srolovitz DJ. Philos Mag B 1989;59:293–329.

[13] Glazier JA. Phys Rev Lett 1993;70(14):2170–713.

[14] Zollner D, Streitenberger P. Scripta Mater 2006;54(9):1697–702.

[15] Thomas GL, de Almeida RMC, Graner F. Phys Rev E 2006;74(2).

[16] Kim YJ, Hwang SK, Kim MH, Kwun SI, Chae SW. Mater Sci Eng A – Struct 2005;408(1–2):110–20.

[17] Ivasishin OM, Shevchenko SV, Semiatin SL. Acta Mater 2009;57(9):2834–44.

[18] Geiger J, Roosz A, Barkoczy P. Acta Mater 2001;49(4):623–9.

[19] Raabe D. Ann Rev Mater Res 2002;32:53–76.

[20] Ding HL, He YZ, Liu LF, Ding WJ. J Cryst Growth 2006;293:489–97.

[21] Krill CE, Chen LQ. Acta Mater 2002;50(12):3057–73.

[22] Moelans N, Wendler F, Nestler B. Comput Mater Sci 2009;46(2):479–90.

[23] Ginzburg VL, Landau LD. Zh Eksperim Teor Fiz 1950;20:1064–82.

[24] Dorr MR, Fattebert JL, Wickett ME, Belak JF, Turchi PEA. J Comput Phys 2010;229(3):626–41.

[25] McKenna I, Gururajan M, Voorhees P. J Mater Sci 2009;44:2206–17.

[26] Kim SG, Kim DI, Kim WT, Park YB. Phys Rev E 2006;74(6):61605.

[27] Xuea X, Righettia F, Telleya H, Lieblinga TM, Mocellin A. Philos Mag B 1997;75(4):567–85.

[28] Nagai T, Ohta S, Kawasaki K, Okuzono T. Phase Transit 1990;28:177–211.

[29] Fuchizaki K, Kusaba T, Kawasaki K. Philos Mag B 1995;71:333–57.

[30] Weygand D, Brechet Y, Lepinoux J, Gust W. Philos Mag B 1999;79(5):703–16.

[31] Williams WM, Smith CS. Trans Am Inst Min Met Eng 1952;194:755–65.

[32] Smith CS. Metall Rev 1964;9(1):1–48.

[33] Wakai F, Enomoto N, Ogawa H. Acta Mater 2000;48(6):1297–311.

[34] Brakke K. Exp Math 1992;1:141–65.

[35] Kuprat A, George D, Straub G, Demirel MC. Comput Mater Sci 2003;28(2):199–208.

[36] Barrales-Mora LA, Gottstein G, Shvindlerman LS. Acta Mater 2008;56(20):5915–26.

[37] Syha M, Weygand D. Model Simul Mater Sc 2010;18:015010.

[38] Lazar EA, MacPherson RD, Srolovitz DJ. Acta Mater 2010;58(2):364–72.

[39] Townsend SJ, Frost HJ, Nichols CS. Mechanisms of grain growth in bubble-fence-delineated films. In: Fluss MJ, Kee RJ, Srolovitz DJ, Volkert CA, editors. Modeling and simulation of thin-film processing; 1995. p. 143–8.

[40] Glicksman ME. Philos Mag 2005;85(1):3–31.

[41] Rhines FN, Craig KR, DeHoff RT. Metall Trans 1974;5(2):413–25.

[42] Ferro AC, Fortes MA. Interface Sci 1997;5(4):263–78.

[43] Glazier JA, Weaire D. J Phys: Condens Mater 1992;4(8):1867–94.

[44] Meijering JL. Philips Res Rep 1953;8:270–90.

[45] Kusner R. Proc Roy Soc A – Math Phys 1992;439(1907):683–6.

[46] DeHoff RT. Acta Metall Mater 1994;42(8):2633–43.

[47] Coxeter HSM. Illinois J Math 1958;2(4B):746–58.

[48] Saito Y. ISIJ Int 1998;38(6):559–66.

[49] Grünbaum B. Convex polytopes. London: Interscience; 1967.